Chemical Physics 91 (1984) 141–159
North-Holland, Amsterdam



# DETERMINATION OF RATES OF COLLISION-INDUCED VIBRATIONAL AND INTRAMULTIPLET TRANSITIONS FOR YO($A^2\Pi$) MOLECULES IN Ar- AND $N_2$-DILUTED FLAMES

T. WIJCHERS, H.A. DIJKERMAN, P.J.Th. ZEEGERS and C.Th.J. ALKEMADE

*Fysisch Laboratorium der Rijksuniversiteit Utrecht, Postbus 80000, 3508 TA Utrecht, The Netherlands*

Received 27 December 1983; in final form 26 April 1984

Rate constants for single-step collisional transitions between specified vibrational and electronic-doublet levels of YO($A^2\Pi$) molecules were determined under multiple-collision conditions at constant total gas pressure. We recorded simultaneously the thermal emission spectrum and the fluorescence spectra induced by a cw dye laser tuned successively at various vibronic transitions. We used premixed $N_2$-diluted or Ar-diluted $H_2$–$O_2$ flames at 1 atm and $\approx 2350$ K, containing YO vapour. Relative rate constants (normalized to the quenching plus radiative de-excitation rate constant) were obtained by solving a set of simultaneous master equations involving the stationary laser-induced population increments. Absolute rate constants were derived therefrom by determining indirectly the fluorescence efficiency. Exoergic doublet-mixing collisions appeared to have greater probabilities than $\Delta v = -1$ or $-2$ transitions and were about equally probable as quenching collisions. Ar and $N_2$ were about equally efficient as collision partner. The rate constants of each process and of its reverse were compared with detailed-balance. The rotational levels in the pumped band appeared to preserve the e/f symmetry index partially.

## 1. Introduction

When a diatomic molecule M in a gas of perturber atoms A is optically pumped from the ground state into a selected level $p$ of an excited electronic state, the fluorescence spectrum depends on the competition between collisional relaxation and emission. The total fluorescence intensity from the excited electronic state depends on the rate at which molecules are transferred by collisions from that state to the ground state (quenching) or other electronic states (intermultiplet transfer). The distribution of the fluorescence over the rotational lines and vibrational bands depends on the rates of rotational and vibrational energy transfer (RET and VET) within the excited state. The distribution of the fluorescence over the spectral components of an excited multiplet is governed by the rate of intramultiplet energy transfer, spin–orbit relaxation or multiplet-mixing, for short. At pressures of $\approx 1$ atm or lower these relaxation processes occur mainly by binary collisions between M and a single perturber atom.

The frequency of a binary collision process that transfers molecules from level $i$ to level $j$ is given by the (apparent monomolecular) *rate constant* $k_{ij}$. It is the probability per second (in $s^{-1}$) that a given molecule in level $i$ is transferred to level $j$ by a single collision. This rate constant is proportional to the number density (= number per unit volume) of the perturber atoms. The rate constants are related to the interaction forces between the molecule in the excited state and the perturber, which are of fundamental interest. Knowledge of the rate constants for inelastic collisions is also of practical interest in the application of fluorescence to the diagnostics of gaseous systems and to spectrochemical analysis [1,2]. This is especially true when one wants to attain optical saturation.

We applied the stationary fluorescence method to study VET and multiplet-mixing processes of YO molecules that were selectively pumped by a tunable cw dye laser to a vibrational level of one of the $A^2\Pi_{1/2,3/2}$ doublet states. Free YO molecules were produced at a trace concentration in a premixed $H_2$–$O_2$ flame diluted by Ar or $N_2$ at

0301-0104/84/$03.00 

1 atm total pressure, into which an yttrium salt solution was nebulized [1]. The composition of the flame was such that the main perturbers were Ar or $N_2$ and $H_2O$. The equilibrium population distribution could be observed in the spectrum of the thermal $A^2\Pi \rightarrow X^2\Sigma$ emission bands. The deviation from the equilibrium distribution under pumping conditions was measured by analyzing the corresponding fluorescence bands. The perturbed population distribution is related to the rate constants of collisional energy transfer between the pumped and the other observed levels. By tuning the laser frequency we were able to pump several vibrational levels in the $A^2\Pi_{1/2,3/2}$ states. From this set of perturbed population distributions we determined relative rate constants for single-step $(v, \Omega)$ transitions under *multiple*-collision conditions. By determining indirectly the quantum efficiency of fluorescence and using the known optical lifetime, we also obtained the absolute rate constants.

We chose the YO molecule as object of our study because (i) the absorption bands of the $A^2\Pi \leftarrow X^2\Sigma$ transition lie in the visible range covered by the powerful rhodamine 6G dye laser, (ii) the vibrational bands are well separated, whereas the Franck–Condon factors of the $A^2\Pi \leftarrow X^2\Sigma$ transition are close to unity for $\Delta v = 0$ [3], (iii) the molecular constants and designation of the levels involved are well-known [4,5], (iv) the $A^2\Pi$ state has a significant doublet splitting, enabling us to measure mixing rate constants, (v) the optical lifetime of this state is well-known [3] and short enough to ensure a reasonable efficiency of fluorescence [1] in flames at 1 atm pressure, and (vi) in the flame yttrium monoxide is a stable compound because of its high dissociation energy [6].

A premixed, shielded combustion flame combined with a pneumatic nebulizer offers the following advantages: (i) it provides a simple means of producing a uniform vapour of YO molecules, (ii) the existence of thermal equilibrium in the flame gas allows us to compare the rate constants of each process and time-reversed process with the detailed-balance relation [1], (iii) the observation of the thermal YO($A^2\Pi$) emission (in the absence of laser pumping) enables us to eliminate the Franck–Condon factors and spectral sensitivity of the spectrometer in the evaluation of our fluorescence experiments, and (iv) the high flame temperature $T$ enables us to pump a fairly large number of vibrational levels by $\Delta v = 0$ transitions from the ground state (the vibrational energy quantum is $\approx \frac{1}{2}k_B T$, where $k_B$ is Boltzmann's constant).

Disadvantages of the flames used are: (i) $H_2O$ molecules play a constant but unknown role in the relaxation studied, (ii) the relaxation time for the equilibration of the rotational degree of freedom is, on the one hand, too short to study RET collisions and, on the other hand, too long to ensure a partial Boltzmann distribution over the rotational levels when a single rovibronic level is pumped, and (iii) the flame gas pressure cannot easily be varied. In the following sections we shall describe how these disadvantages were dealt with in our experiments.

Quantitative experiments on VET and doublet-mixing processes of excited YO molecules have not yet been reported in the literature. A few qualitative observations on these processes have been reported by Linton [7] as a by-product of his investigation on the YO($A^2\Pi \rightarrow X^2\Sigma$) fluorescence spectrum. The YO molecules were formed by the $Y + O_2$ reaction in a low-pressure Ar-flow system. In similar flow systems, quantitative fluorescence experiments on RET and VET have been done mainly with BaO($A^1\Sigma$) molecules [8–10]. Multiplet-mixing experiments have been done, for example, with electronically excited CdH [11] and BaCl molecules [12,13]. A preliminary description of our YO($A^2\Pi$) fluorescence experiments has been published in ref. [14], whereas a full account has been given in ref. [15].

The aim of the present article is to demonstrate the possibility of extracting rate constants for single-step transitions between $(v, \Omega)$-levels of YO($A^2\Pi$) molecules under multiple-collision conditions at constant total gas pressure. The results obtained in flames will be reported in section 5 and discussed in section 6.

## 2. Theoretical basis

### 2.1. Spectrum

The visible spectrum of the YO molecule has been known for a long time [4,16]. It involves only a few electronic states, viz. the $X\,^2\Sigma^+$ ground state and the $A'\,^2\Delta$, $A\,^2\Pi$ and $B\,^2\Sigma^+$ states in order of increasing excitation energy. The corresponding transitions to the ground state lie in the red, orange–red and blue–green part of the spectrum, respectively. A very weak emission from the $A'\,^2\Delta$ state has been reported more recently [17]. Due to admixture of the neighbouring $A\,^2\Pi$ state the optical selection rules ar slightly relieved for this transition. Some spectroscopic constants are given in table 1, which also explains the short-hand notation (X, $A_1$, $A_2$,) used in the present paper for the electronic states of direct interest. We note in the table the considerable spin–orbit splitting of 428 $cm^{-1}$ of the $A\,^2\Pi$ state, which belongs to Hund's case a for most rotational levels that are markedly populated at our flame temperature [5].

Because the potential curves of the $A_{1,2}$ and X states lie almost vertically above each other, the orange–red bands are mainly grouped in two strong $\Delta v = 0$ sequences, characterized by $\Omega = 1/2$, $3/2$. Spin–orbit splitting in the X state is negligible [4]. $\Lambda$-doubling is appreciable in the $A_1$ state but negligible in the $A_2$ state [4]. Consequently, only four of the six possible branches are distinguishable in each doublet-subsystem; two pairs of branches (e.g., $P_1$ and $Q_{12}$) coincide. The designation of these branches and of their combinations (P, Q and R) is given in table 2. This table also lists the approximated theoretical intensity ratios of the P-, Q- and R-emission lines having a common lower rotational quantum number $J''$. These ratios apply for not too low $J$-values when the upper $J'$ levels and the sublevels of the $\Lambda$-doublets are equally populated (see section 6.3). With respect to the rather sharply peaked Q-branch, the P-branch extends to longer wavelengths (increasing with increasing $J'$), whereas the R-branch extends to shorter wavelengths.

Table 2
Branches of $A_{1,2}$–X transitions

| | P-branch | Q-branch | R-branch |
|---|---|---|---|
| $A_1$–X | $P_{12}$: $(P_1 + Q_{12})$ | $(Q_1 + R_{12})$ | $R_1$ |
| $A_2$–X | $P_2$: $(P_{21} + Q_2)$ | $(Q_{21} + R_2)$ | $R_{21}$ |
| intensity ratios [a] | $(1 \div 3)$ | 3 | 1 |

[a] According to ref. [5].

### 2.2. Rate equations

#### 2.2.1. General

We assume that in the absence of laser pumping all level populations conform to Boltzmann equilibrium. We also assume that the collisional rate constants measured are unaffected by the pumping rate and are equal to the thermal rate constants that apply in thermal equilibrium. We note that the pumping process affects only the relative distribution of the YO molecules over their internal states and that YO–YO collisions are negligible. Between the thermal rate constant $k_{ij}(T)$ of an inelastic collision process that transfers the molecule from level $i$ to level $j$, and the thermal rate constant $k_{ji}(T)$ of the time-reversed process we

Table 1
Spectroscopic constants of YO ($cm^{-1}$)

| State | Short symbol | $T_e$ | $\omega_e$ | $\omega_e x_e$ | $B_e$ | $\alpha_e$ |
|---|---|---|---|---|---|---|
| $X\,^2\Sigma^+$ [a] | X | 0 | 862.0 | 2.86 | 0.3889 | 0.0017 |
| $A'\Delta_{3/2}$ [b] | A' | 14531.2 | 794.0 | 3.23 | 0.3761 | 0.0017 |
| $A'\Delta_{5/2}$ [b] | A' | 14870.4 | 794.9 | 3.3 | 0.3761 | 0.0017 |
| $A\,^2\Pi_{1/2}$ [b] | $A_1$ | 16315.8 | 823.0 | 3.45 | 0.3865 | 0.0019 |
| $A\,^2\Pi_{3/2}$ [b] | $A_2$ | 16746.8 | 820.0 | 3.38 | 0.3865 | 0.0019 |
| $B\,^2\Sigma^+$ [a] | B | 20741.9 | 765.0 | 7.75 | 0.3732 | 0.0025 |

[a] See ref. [5]. [b] See ref. [17].

have the *detailed-balance relation* [1]:

$$k_{ij}(T)/k_{ji}(T) = n_j^e/n_i^e. \quad (2.1)$$

Here $n_i^e$ and $n_j^e$ are the thermal equilibrium populations of level $i$ and $j$, respectively, which obey the Boltzmann distribution law.

Let the indices $i$, $j$ denote any pair out of a selected group, S, of $N$ ($\Omega$, $v$)-levels that belong to the $A_1$ or $A_2$ state, for which we want to determine the rate constants $k_{ij}$. Let index $q$ denote any level of the rest group, Q, of electronically excited levels that do not belong to S, and $g$ any ground-state level. The increment, $\delta n_i$, in the number density $n_i$ (= number per unit of volume) of molecules in level $i$ is related to the (positive or negative) increments in the other level populations for given pumped level by the master equation

$$\sum_{j=1}^{N}(k_{ji} + A_{ji})\delta n_j + \sum_q (k_{qi} + A_{qi})\delta n_q + \sum_g k_{gi}\delta n_g - \left[\sum_{j=1}^{N}(k_{ij} + A_{ij}) + W_i\right]\delta n_i = 0. \quad (2.2)$$

Here $A_{ji}$ and $A_{qi}$ are the Einstein coefficients (in $s^{-1}$) for a spontaneous transition from level $j$ and $q$, respectively, to level $i$. Of course, when level $i$ lies above level $j$ or $q$, these coefficients are zero. When we define $k_{ii} \equiv 0$ and $A_{ii} \equiv 0$, the summation $\Sigma_{j=1}^{N}$ extends over all $N$ levels of the selected group S. The summations $\Sigma_q$ and $\Sigma_g$ extend over all levels $q$ and $g$, respectively. The coefficient $W_i$ denotes the sum of all rate constants of collisional and radiative transitions from level $i$ to any rest level $q$ or ground level $g$. For $i = p$ we would have to add to eq. (2.2) a term describing the pumping rate. Since this rate could not be measured, we suppose $i \neq p$ in this equation.

For each choice of pumped level $p$ (called: pumping mode), we now have a set of $(N-1)$ linear master equations of the form of eq. (2.2) with $i = 1,\ldots,N$ but $\neq p$. It is our general aim to derive the $k_{ij}$ values from the measured relative population increments by solving a sufficiently large number of such sets of equations, each set corresponding to a different pumping mode.

It may happen for some pairs of levels that even under pumping conditions the *ratio* of their populations, $n_i/n_j$, equals (approximately) the Boltzmann ratio $n_i^e/n_j^e$ although each $n_i$ and $n_j$ deviates from $n_i^e$ and $n_j^e$, respectively. It follows immediately that then also $\delta n_i/\delta n_j$ equals $n_i^e/n_j^e$. *Partial* Boltzmann equilibrium is then said to exist between this pair of levels. Using eq. (2.1) we immediately see that the terms $k_{ji}\delta n_j$ and $k_{ij}\delta n_i$ occurring in the master equation then cancel each other (approximately).

### 2.2.2. *Numerical solution*

Even when we try to solve an extensive set of simultaneous master equations by numerical methods, the number of unknowns may still exceed the number of independent observables. We shall therefore simplify eq. (2.2) by introducing some approximations.

(i) We can safely neglect all terms involving non-zero Einstein coefficients for spontaneous transitions *between* excited states in comparison with the term $W_i\delta n_i$ which involves a spontaneous transition from level $i$ to the ground state with a rate coefficient as large as $3 \times 10^7$ $s^{-1}$ [3]. (ii) The term $\Sigma_g k_{gi}\delta n_g$ describing the collisional excitation from the ground state can be safely neglected. This holds because – according to the detailed-balance relation, eq. (2.1) – $k_{gi}$ is much smaller than $k_{ig}$, which is contained in $W_i$, whereas $\Sigma\,\delta n_g$ and the relevant $\delta n_i$ values are of comparable order of magnitude. (iii) We will introduce an effective, overall rate constant $k_{Qi}$ defined by

$$k_{Qi} \equiv \sum_q k_{qi}\delta n_q / \sum_q \delta n_q. \quad (2.3)$$

The total population increment of the rest group, $\delta n_Q \equiv \Sigma_q\,\delta n_q$, is not known as we did not detect any radiation from the A′ state. We can, however, estimate from fluorescence measurements the contributions to $\delta n_Q$ made by levels of the B and A states. We shall denote the latter two contributions by $(\delta n_Q)_B$ and $(\delta n_Q)_A$, respectively. Expressing the ratio between the contribution from the A′ levels, $(\delta n_Q)_{A'}$, and $(\delta n_Q)_B$ by an, as yet unspecified factor $\xi$, we have

$$\delta n_Q \equiv \sum_q \delta n_q = (\delta n_q)_A + (\delta n_q)_B(1+\xi). \quad (2.4)$$

With the above simplifications and assumptions the master equation (2.2) reduces to

$$\sum_{j=1}^{N} k_{ji}\delta n_j + k_{Qi}\delta n_Q - \left(\sum_{j=1}^{N} k_{ij} + W_i\right)\delta n_i = 0. \tag{2.5}$$

This equation relates, for given $p$, the measured $\delta n_j/\delta n_i$ ratios and estimated $\delta n_Q/\delta n_i$ ratio to the rate constants $k_{ij}$ sought.

In order to render the calculations tractable we shall assume that the unknown $\xi$ [contained in eq. (2.4)] does not depend markedly on the pumping mode $p$.

The ratios of the population increments, $\delta n_j/\delta n_i$, can be found from the intensity ratios of the fluorescence and thermal emission of the corresponding vibrational bands, $\delta I_i/I_i^e$ and $\delta I_j/I_j^e$. We have, in the absence of self-absorption and saturation effects

$$\delta n_i/n_i^e = \delta I_i/I_i^e, \quad \text{etc.}, \tag{2.6}$$

and thus

$$\frac{\delta n_j}{\delta n_i} = \frac{\delta I_j}{\delta I_i}\frac{I_i^e}{I_j^e}\frac{n_j^e}{n_i^e}. \tag{2.7}$$

The equilibrium population ratio can be calculated from the Boltzmann distribution law at known flame temperature according to

$$n_j^e/n_i^e = (g_j/g_i)\exp(-E_{ji}/k_B T), \tag{2.8}$$

where $g_j$ and $g_i$ are the statistical weights, $E_{ji}(\equiv E_j - E_i)$ is the difference of excitation energies of levels $j$ and $i$. Expression (2.8) is strictly valid also when we disregard the *rotational* degree of freedom, i.e. when $n_i^e$, etc., relates to the total equilibrium population of the $i$th $(v, \Omega)$-level, summed over all rotational levels. In that case, $E_i$ etc., refers to the well-defined excitation energy of the *lowest* rotational level in the considered $(v, \Omega)$-level. We note that in this spectroscopic determination of the relative population increments, the Franck–Condon factors, the spectral sensitivity of the spectrometer and the observation volumes in the fluorescence and thermal emission measurements drop out. Also the pumping rate drops out.

In order to solve $M$ sets of $(N-1)$ independent linear equations, obtained with $M$ different pumping modes, the number of unknowns must not exceed $M(N-1)$. In order to relax this condition we shall ad hoc assume that $W_i$ is a constant, $W$, independent of $i$ (i.e., the radiative and quenching rate constants are the same for all vibrational levels concerned). Furthermore, we shall content ourselves with solving for the *normalized* rate constants $k_{ij}/W$. In this way the number of unknowns is restricted to $N^2$. We shall later test this assumption and determine $W$ from the experimental efficiency of fluorescence.

### 2.2.3. Solution by successive approximation

As an extra check on the numerical results we will introduce here a more straightforward but cruder solution method which is based on successive approximation and involves much simpler equations. Although the accuracy of this method may be inferior to that of the numerical method, this cross-examination may detect serious systematic errors possibly made.

In first approximation we consider, in addition to the pumped level $p$, only a single neighbouring level $i$. Level $i$ may be the vibrational level that is next (below or above) to the pumped level $p$ belonging to the same doublet component or it may be the same vibrational level belonging to the other component. We assume that level $i$ is populated only by a single collisional transition from level $p$ with rate constant $k_{pi}$. The overall depopulation rate constant $R$ is supposed to be, virtually, independent of $i$. [We note that this $R$ differs from $W_i$ introduced in eq. (2.2).] Then, under stationary pumping conditions, the balance equation reads in first approximation [denoted by affix (1)]:

$$k_{pi}^{(1)}\delta n_p = R\delta n_i. \tag{2.9}$$

From this equation we find $k_{pi}^{(1)}/R$, by using the measured $\delta n_i/\delta n_p$ ratio, for each of the three abovementioned neighbouring levels $i$. By choosing a set, $T$, of successive levels as pumped level $p$ we obtain in this way a coherent set of $k_{ij}^{(1)}/R$ ratios for all neighbouring level pairs $(i, j)$ belonging to set $T$. Using these first-order ratios, we can find second-order ratios $k_{pi}^{(2)}/R$ from the extended

balance equation

$$k_{pi}^{(2)}\delta n_p + \sum_j k_{ji}^{(1)}\delta n_j = R\delta n_i. \qquad (2.10)$$

where $i$ is a neighbouring level of pumped level $p$ and the summation extends over the two remaining neighbouring levels of $i$. By varying $p$, as before, we obtain a set of $k_{ij}^{(2)}/R$ ratios in second-order approximation. This procedure can be repeated to obtain a third-order approximation $k_{ij}^{(3)}/R$, and so on, until the series converges sufficiently.

## 3. Experimental details

### 3.1. Experimental arrangement and measuring conditions *

#### 3.1.1. Flame and nebulizer

The premixed, oxygen-rich $H_2$–$O_2$–Ar and $H_2$–$O_2$–$N_2$ flames at 1 atm pressure and with temperatures of 2420 ± 15 and 2290 ± 5 K, respectively, were produced by a Méker-grid burner [1]. The burnt gas composition was: ≈ 50% Ar or $N_2$, 40% $H_2O$ and ≈ 7% ($CO_2$ + CO); the latter constituents were due to the combustion of the solvent. The temperatures were measured by the usual line-reversal method using the Na-*D* lines and agreed with the vibrational temperatures measured on the Q-branches of the thermal (A–X, $\Delta v = 0$) emission. By scanning the laser wavelength over the (A, $v' = 0 \leftarrow$ X, $v'' = 0$) absorption band and measuring the total fluorescence intensity we found that the rotational temperatures in the ground-state also agreed with the above values. The rotational level populations in this state were independent of the pumping rate.

A pneumatic nebulizer (Varian Techtron) was attached to the centre of the burner bottom. It fed the central flame with an aerosol of an yttrium–perchlorate solution in ethanol, containing 0.6 g/ℓ yttrium.

#### 3.1.2. Q-branch pumping

A cw laser (Coherent Radiation model 590) with rhodamine 6G dye, pumped by an $Ar^+$ laser (Spectra Physics model 171) at 514 nm, was used to pump a selected vibronic level of the $A_{1/2}$-states. We chose the Q-branch of the (A ← X, $\Delta v = 0$) absorption band for pumping. The laser bandwidth $\Delta\lambda_L$ was 0.06 nm and the laser power was ≈ 200 mW. The laser beam was retro-reflected 10 times so that the effective absorption path length was 8.3 cm (see fig. 1). The incident laser power was monitored by detector $D_2$ connected to ac voltmeter V.

Since the thermal rate constants to be measured are averaged over the rotational distribution in the initial ($v$, $\Omega$)-level, it is essential that the relative rotational distribution obeys Boltzmann's law at flame temperature $T$. The rotational distribution in the ground state was known to be thermal (see section 3.1.1). Then excitation by radiation with *relative* spectral distribution conforming to Planck's law at temperature $T$, would produce a thermal relative rotational distribution in the excited state if the population of this state was radiation-dominated. This holds because of detailed-balance considerations, irrespective of the variation of the absorption line strength with $J''$. We now assume that a thermal relative rotational

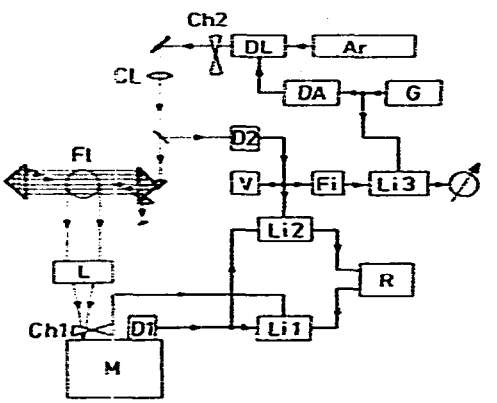


Fig. 1. Block scheme of the complete arrangement for excitation, fluorescence and thermal emission measurements. Ar = argon-ion laser; DL = dye laser; DA = driving amplifier; G = generator; Ch1 and Ch2 = chopper; CL = collimating lens; Fl = flame; L = imaging system; M = monochromator; D1 and D2 = photon-detector; Li1, Li2 and Li3 = lock-in amplifier; V = voltmeter; Fi = low-pass filter; R = two-channel stripchart recorder.

* For more details we refer to refs. [14,15].

distribution in the pumped ($v$, $\Omega$)-level is, approximately, also attained when we pump only the Q-branch of that level with a quasi-white light source. (The variation of the Planck factor with wavelength within the width $\delta\lambda_Q$ of the Q-branch is negligible, as $\Delta\lambda_Q$ is at most 0.5 nm.) Since the actual laser bandwidth $\Delta\lambda_L$ was much smaller than $\Delta\lambda_Q$, we simulated a quasi-white excitation within $\Delta\lambda_Q$ by sweeping the laser wavelength, at constant laser power $P_L$, over a range $\Delta\lambda_s = \Delta\lambda_Q$ at a uniform rate with a repetition frequency of 5 Hz. This was achieved by equipping the laser cavity with an etalon-tilting device which was driven by signal generator G (see fig. 1) [15]. The *time-averaged* fluorescence spectrum from the pumped ($v$, $\Omega$)-level can then be shown [15] to be the same as with a broad-band (quasi-white) laser with $\Delta\lambda'_L = \Delta\lambda_s$ and uniform spectral power $(P'_L)_\lambda = P_L/\Delta\lambda_s$. We shall discuss later how well the condition of a thermal rotational distribution was fulfilled in the observed ($v$, $\Omega$)-levels.

### 3.1.3. Registration of the fluorescence and thermal emission spectra

The laser-excited fluorescence and thermal emission spectra were recorded with scanning monochromator M (0.2 nm/min; bandwidth ≈ 0.15 nm). The fluorescence spectrum was recorded through lock-in Li2 by chopping the laser radiation at 125 Hz by a mechanical chopper Ch2. The combined fluorescence and thermal emission was recorded through Li1 by chopping the light beam entering the monochromator at 260 Hz by Ch1 (see fig. 1). The fluorescence intensities turned out to be much smaller than the thermal intensities. The fluorescence and thermal emission spectra were recorded simultaneously on a two-channel stripchart recorder R. The overall response time was long compared to the sweep period of the laser-wavelength modulation. The fluctuations in the fluorescence measurements were mainly due to thermal emission noise. For a full description we refer to refs. [14,15].

### 3.2. Experimental procedures

The strong, wavelength-integrated, Q-branches of the fluorescence and thermal emission ($\Delta v = 0$) bands were selected as a measure for $\delta I$ and $I^e$, respectively. Wavelength-integration was performed with an electronic planimeter (HP 9864A). We corrected for the underlying wings of the P- and R-branches by interpolating these wings with a straight baseline. The experimental error in $\delta I/I^e$ was at most ≈ 10% [15].

In the measurement of the fluorescence emitted from the pumped level itself, we recorded a $\Delta v = +1$ or $-1$ transition in order to avoid contamination by straylight from the laser. The $\delta I$ values so obtained were compared with the $I^e$ values corresponding to the same $\Delta v$ transition. This procedure was not possible when the $v' = 0$ level of the $A_2$ state was pumped, because of overlap of the $v' = 0 \rightarrow v'' = 1$ band with strong, collisionally induced $\Delta v = 0$ bands from the other doublet component. Therefore we observed the $v' = 0 \rightarrow v'' = 0$ band in fluorescence and corrected for straylight as described in ref. [15].

The integrated Q-branches measured in fluorescence and thermal emission are an unambiguous measure for the laser-induced and thermal populations, respectively, only if the *ratios* between their integrated P-, Q- and R-branches are the same. The branch ratios of the fluorescence bands from the collisionally populated vibrational levels $i$ ($\neq p$) were found to be the same as in thermal equilibrium (namely P : Q : R = 4 : 3 : 1; see table 2). This was not the case, however, for the band emitted by the pumped level $p$. For the pumped $v = 0$ level we measured branch ratios P : Q : R = 1.7 : 3 : 0.4 in the Ar-diluted flame and P : Q : R = 1.3 : 3 : 0.3 in the $N_2$-diluted flame. Since the extent of these deviations is not likely to depend on $v$ (see section 6.3), we assumed that these branch ratios hold for all pumped levels. We applied accordingly a same *Q-branch correction factor* for all pumped levels in a given flame.

In those cases where P-, Q- or R-branches could be observed in fluorescence free from overlap by other, stronger bands, their individual shapes were checked to be similar as in thermal emission. This was also the case for the branches belonging to the pumped level if the laser spectrum was made broad-banded by sweeping its wavelength across the Q-branch. (With a narrow-band laser at fixed wavelength this was clearly not the case [14,15].)

This outcome supports our assumption in section 3.1.2 that the relative rotational distribution in all observed ($v$, $\Omega$)-levels was close to thermal also under pumping conditions. We, finally, checked that the fluorescence radiation was unpolarized and optical saturation was absent.

Another correction, called *overlap correction*, dealt with the partial overlap of the Q-branch used in pumping level $p$, by P- and R-branches of neighbouring $\Delta v = 0$ absorption bands. Because of this overlap we pumped not only level $p$ but also, unintentionally, other levels $k$ (which may even include the observed level $i$, but not $p$). Consequently, the laser-induced fluorescence from level $i$, $(\delta I_i)_p$, observed with the laser tuned to the Q-branch of $p$, contained contributions, $(\delta I_i)_{pk}$, due to overlap of this branch with the P- or R-branches of $k$:

$$(\delta I_i)_p = (\delta I_i)_{pp} + \sum_k (\delta I_i)_{pk}. \qquad (3.1)$$

Here $(\delta I_i)_{pp}$ is the wanted contribution due to pumping of level $p$ alone. We corrected for these spurious pumping contributions by successive approximation as described in ref. [15].

## 4. Spectroscopic observations

The vibronic levels that were selected for pumping are listed in table 3, together with the upper levels of the transitions that were observed in fluorescence as well as in thermal emission. The number of pumped levels selected with the $N_2$-diluted flame was less than that with the Ar-diluted flame because, in general, with the former flame weaker signals were obtained.

Fig. 2 shows two typical spectrograms recorded simultaneously in thermal emission and in fluorescence when the Q-branch of the ($A_2$, $v'_p = 0 \leftarrow X$, $v''_p = 0$) band was pumped with the Ar-diluted flame. We checked from the spectrograms that the intensities of the thermal band emissions from the $A_1$- and $A_2$-doublet states were the same within 10% after correction for their different Boltzmann and Franck–Condon factors [3] and for the spectral sensitivity of the spectrometer. The statistical weight factors for the vibronic levels involved are thus the same, as expected theoretically, and drop out in eq. (2.8).

Table 3
Levels selected for pumping and observation

| Pumping levels [a] | Observation levels [a] | $v'-v''$ |
|---|---|---|
| $A_1$ | $A_1$: $v' = 0, 1, \ldots, 8 (\neq v'_p)$ | 0 |
| | $A_1$: $v' = v'_p$ | −1 |
| $v'_p = 0, 1, \ldots, 8$ (Ar) | $A_2$: $v' = 0, 1, \ldots, 8$ | 0 |
| $v'_p = 0, 1, \ldots, 4$ ($N_2$) | B: $v' = 0, 1$ | 0 |
| | B: $v' = 2, 3$ | +1 |
| $A_2$ | $A_1$: $v' = 0, 1, \ldots, 8$ | 0 |
| | $A_2$: $v' = 0, 1, \ldots, 8 (\neq v'_p)$ | 0 |
| $v'_p = 0, 1, \ldots, 7$ (Ar) | $A_2$: $v' = v'_p$ | +1 |
| $v'_p = 0, 1, \ldots, 4$ ($N_2$) | B: $v' = 0, 1$ | 0 |
| | B: $v' = 2, 3$ | +1 |

[a] For explanation of symbols see also table 1; $v'_p$ denotes vibrational quantum number of pumped level. The vibrational transitions from the ground state used in the pumping process obey $\Delta v = 0$; the observed vibrational transitions to the ground state are indicated by $v'-v''$. Symbols (Ar) and ($N_2$) refer to the experiments in the Ar- and $N_2$-diluted $H_2$-flame, respectively.

From the ratios of the integrated, corrected and normalized $\delta I_i$ values to the corresponding $I_i^c$ values we obtained the relative population increments $\delta n_i$, using eqs. (2.7) and (2.8), through:

$$\delta n_i = C(\delta I_i / I_i^c) \exp(-E_{i0}/k_B T). \qquad (4.1)$$

Here $E_{i0}$ is the known excitation energy of the lowest rotational level of level $i$, specified by quantum numbers ($v$, $\Omega$), with respect to that of the lowest rotational level of the A(0, 1/2)-state. The constant of proportionality $C$, which is independent of $i$, contains, among others, the total density of YO molecules and the ratio of the (effective) flame volumes observed in fluorescence and in thermal emission, respectively. We note that this constant drops out when calculating the $\delta n_j/\delta n_i$ ratios through eq. (2.7). The *reduced* $\delta n_i$ values obtained from the observations through eq. (4.1) with $C \equiv 1$ for different pumping modes are collected in tables 4 and 5 for the Ar- and $N_2$-flame, respectively. The error intervals indicated refer only to the uncertainty in the integration of the Q-branches due to noise in the recorded spectra. The last column in these tables lists the $\delta n_Q$ values

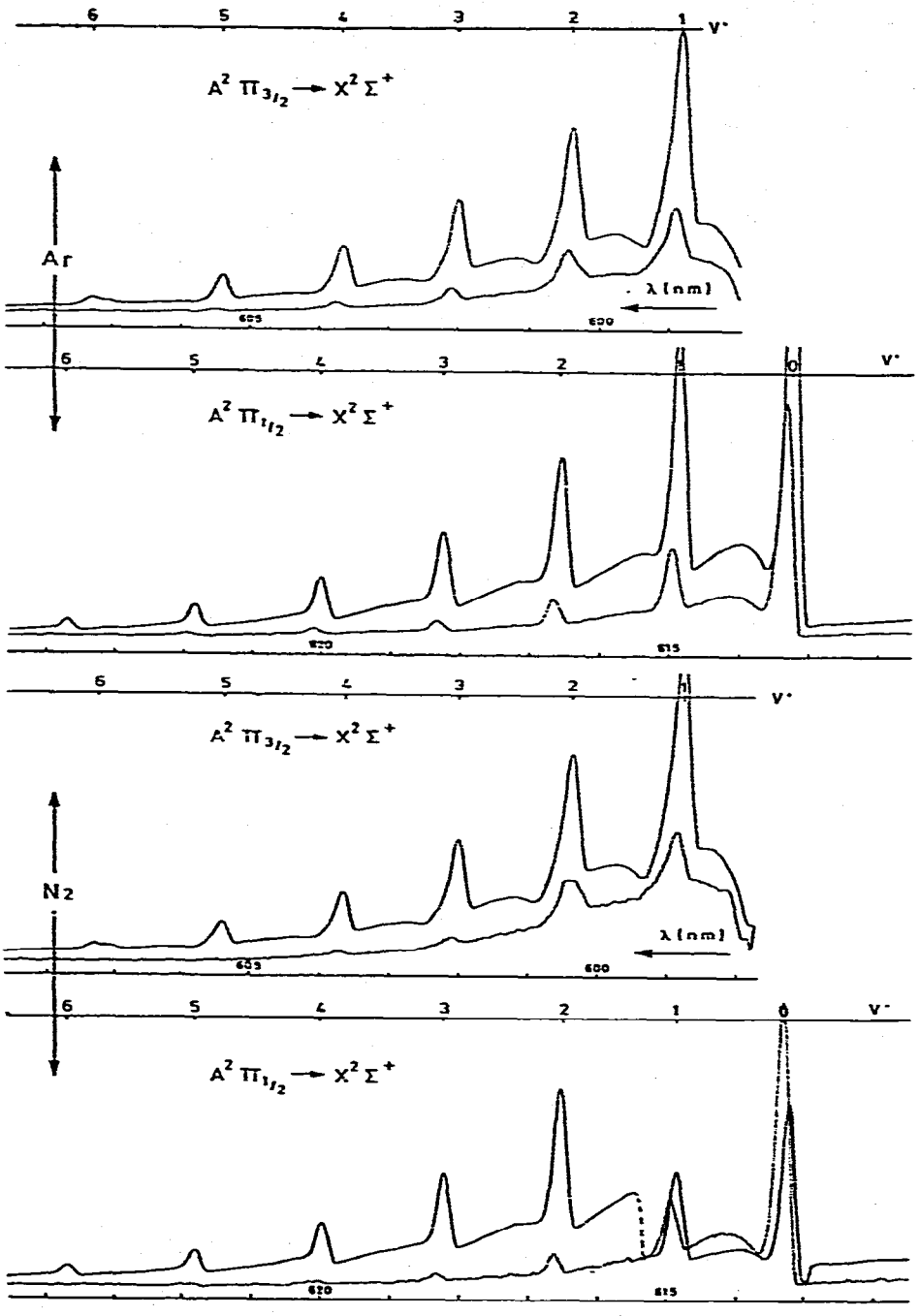


Fig. 2. Example of the simultaneously recorded spectra of fluorescence (lower curve) and the sum of fluorescence and thermal emission (upper curve) of YO in the flame; the $A^2\Pi_{3/2}$, $v = 0$ level was excited by the broad-band laser. The upper part corresponds to the Ar-diluted flame; the lower part shows spectra in the $N_2$-diluted flame. The gain-ratio of the channels leading to the recording of the fluorescence spectrum and the sumspectrum was 5 : 1, except for the lower wavelength-part of the $A^2\Pi_{1/2} \rightarrow X^2\Sigma^+$ spectrum in the $N_2$-diluted flame where this ratio was 15 : 1. The values of $\delta I/I^c$ were determined from similar spectra, but with a much better signal/noise ratio.

Table 4
Reduced population increments $\delta n_v$, obtained through eq. (4.1) from observed $(\delta I_v / I_v^c)$ ratios and normalized to $P_L = 0.2$ Torr and $\Delta\lambda = 0.5$ nm, for different pumping modes ($p$) in the Ar- diluted flame [a]

| | $v_i'$ | 0 | | 1 | | 2 | | 3 | | 4 | | 5 | | 6 | | 7 | | $\delta n_Q$ [b] |
|---|---|---|---|---|---|---|---|---|---|---|---|---|---|---|---|---|---|---|
| $v_p'$ | $\Omega$ | 1/2 | 3/2 | 1/2 | 3/2 | 1/2 | 3/2 | 1/2 | 3/2 | 1/2 | 3/2 | 1/2 | 3/2 | 1/2 | 3/2 | 1/2 | 3/2 | |
| 0 | 1/2 | 20.6 | 10.6 | 3.2 | 2.6 | 1.37 | 1.09 | 0.73 | 0.60 | 0.43 | 0.35 | 0.22 | 0.17 | 0.14 | 0.09 | 0.06 | 0.07 | 5.1 |
| | 3/2 | 11.0 | 16.2 | 3.0 | 2.3 | 1.17 | 0.91 | 0.63 | 0.52 | 0.35 | 0.32 | 0.22 | 0.17 | 0.10 | 0.09 | 0.07 | 0.05 | 4.6 |
| 1 | 1/2 | 4.4 | 2.5 | 6.8 | 4.0 | 1.33 | 0.98 | 0.58 | 0.45 | 0.36 | 0.25 | 0.18 | 0.13 | 0.10 | 0.07 | 0.07 | 0.04 | 3.7 |
| | 3/2 | 3.5 | 5.3 | 4.5 | 12.0 | 1.56 | 1.35 | 0.62 | 0.55 | 0.38 | 0.26 | 0.18 | 0.17 | 0.10 | 0.03 | 0.07 | 0.04 | 5.3 |
| 2 | 1/2 | 1.49 | 1.07 | 2.00 | 1.42 | 4.5 | 2.04 | 0.70 | 0.49 | 0.27 | 0.25 | 0.16 | 0.16 | 0.09 | 0.08 | 0.04 | 0.04 | 2.6 |
| | 3/2 | 1.35 | 1.69 | 1.87 | 1.73 | 2.7 | 7.2 | 1.10 | 0.76 | 0.39 | 0.17 | 0.22 | 0.15 | 0.13 | 0.10 | 0.07 | 0.05 | 2.9 |
| 3 | 1/2 | 0.60 | 0.41 | 0.70 | 0.35 | 0.84 | 0.60 | 2.8 | 0.81 | 0.32 | 0.21 | 0.12 | 0.08 | 0.05 | 0.05 | 0.05 | 0.03 | 1.6 |
| | 3/2 | 0.56 | 0.63 | 0.39 | 0.66 | 0.52 | 0.78 | 1.00 | 3.3 | 0.45 | 0.32 | 0.15 | 0.07 | 0.07 | 0.06 | 0.04 | 0.04 | 2.1 |
| 4 | 1/2 | 0.17 | 0.25 | 0.30 | 0.19 | 0.29 | 0.19 | 0.33 | 0.31 | 1.42 | 0.42 | 0.13 | 0.09 | 0.07 | 0.04 | 0.02 | 0.02 | 1.0 |
| | 3/2 | 0.34 | 0.25 | 0.27 | 0.34 | 0.23 | 0.33 | 0.35 | 0.39 | 0.59 | 2.1 | 0.31 | 0.16 | 0.11 | 0.03 | 0.04 | 0.04 | 1.2 |
| 5 | 1/2 | 0.09 | 0.11 | 0.03 | 0.11 | 0.12 | 0.10 | 0.17 | 0.09 | 0.24 | 0.18 | 0.92 | 0.24 | 0.10 | 0.05 | 0.03 | 0.02 | 0.6 |
| | 3/2 | 0.13 | 0.09 | 0.10 | 0.10 | 0.11 | 0.15 | 0.08 | 0.17 | 0.15 | 0.16 | 0.25 | 1.37 | 0.15 | 0.08 | 0.04 | 0.02 | 0.8 |
| 6 | 1/2 | 0.08 | 0.03 | 0.04 | 0.03 | 0.05 | 0.04 | 0.01 | 0.04 | 0.04 | 0.03 | 0.01 | 0.07 | 0.25 | 0.08 | 0.04 | 0.02 | 0.6 |
| | 3/2 | 0.08 | 0.07 | 0.05 | 0.03 | 0.07 | 0.01 | 0.05 | 0.09 | 0.03 | 0.17 | 0.06 | 0.07 | 0.10 | 0.75 | 0.06 | 0.03 | 0.7 |
| 7 | 1/2 | 0.08 | 0.08 | 0.08 | 0.07 | 0.04 | 0.06 | 0.04 | 0.04 | 0.05 | 0.04 | 0.05 | 0.03 | 0.08 | 0.05 | 0.4 | 0.07 | 0.5 |
| | 3/2 | 0.05 | 0.05 | 0.04 | 0.02 | 0.03 | 0.02 | 0.03 | < 0.01 | 0.02 | < 0.01 | 0.03 | 0.01 | 0.01 | 0.00 | 0.08 | 0.43 | 0.6 |

[a] Estimated relative errors in the doubly, singly and not underlined figures are: > 20%, 5–20% and < 5%, respectively.
[b] The total, reduced population increment of the rest levels, $\delta n_Q$, was estimated as described in the text.

as defined by eq. (2.4) and again reduced according to eq. (4.1) with $C = 1$. These values were estimated from fluorescence and thermal emission measurements on (B–X) and (A–X) bands combined with extrapolations to the higher lying, unobserved levels. In this extrapolation we assumed partial Boltzmann equilibrium between the highest level observed in fluorescence and the higher lying, unobserved levels. (Partial Boltzmann equilibrium was found to exist already between the highest observed levels.) The contribution of the unobserved A′ levels to $\delta n_Q$ was estimated by setting $\xi$ [defined in eq. (2.4)] equal to the ratio 2 : 1 of the statistical weights of the A′- and B-states.

Table 5
Reduced population increments $\delta n_i$ in the $N_2$-diluted flame; for further legends see table 4

| | $v'_1$ | 0 | | 1 | | 2 | | 3 | | 4 | | 5 | | 6 | | $\delta n_Q$ |
|---|---|---|---|---|---|---|---|---|---|---|---|---|---|---|---|---|
| $v'_P$ | $\Omega$ | 1/2 | 3/2 | 1/2 | 3/2 | 1/2 | 3/2 | 1/2 | 3/2 | 1/2 | 3/2 | 1/2 | 3/2 | 1/2 | 3/2 | |
| 0 | 1/2 | 27.0 | 8.2 | 2.5 | 2.1 | 0.74 | 0.60 | 0.41 | 0.29 | 0.23 | 0.14 | 0.13 | 0.09 | 0.04 | 0.12 | 5.1 |
| | 3/2 | 12.1 | 25.0 | 2.3 | 2.00 | 0.69 | 1.42 | 0.40 | 0.19 | 0.24 | 0.18 | 0.12 | 0.10 | 0.09 | 0.07 | 4.6 |
| 1 | 1/2 | 4.0 | 2.5 | 16.9 | 5.1 | 1.05 | 0.77 | 0.38 | 0.32 | 0.35 | 0.18 | 0.13 | 0.10 | 0.13 | 0.07 | 3.7 |
| | 3/2 | 2.5 | 4.0 | 5.1 | 13.2 | 1.19 | 0.89 | 0.40 | 0.55 | 0.17 | 0.21 | 0.13 | 0.09 | 0.03 | 0.05 | 5.3 |
| 2 | 1/2 | 1.37 | 0.55 | 1.52 | 0.94 | 8.8 | 2.3 | 0.52 | 0.41 | 0.16 | 0.19 | 0.11 | 0.06 | 0.16 | 0.05 | 2.6 |
| | 3/2 | 0.46 | 1.95 | 1.29 | 2.0 | 3.1 | 9.8 | 0.95 | 0.80 | 0.27 | 0.25 | 0.10 | 0.08 | 0.11 | 0.06 | 2.9 |
| 3 | 1/2 | 0.51 | 0.34 | 1.07 | 0.35 | 1.25 | 0.81 | 5.5 | 1.32 | 1.18 | 0.38 | 0.15 | 0.12 | 0.06 | 0.05 | 1.6 |
| | 3/2 | 0.41 | 0.49 | 0.29 | 0.71 | 0.73 | 1.05 | 1.71 | 4.6 | 0.63 | 0.41 | 0.16 | 0.20 | 0.03 | 0.07 | 2.1 |
| 4 | 1/2 | 0.19 | 0.06 | 0.23 | 0.21 | 0.37 | 0.19 | 0.58 | 0.32 | 2.2 | 0.59 | 0.24 | 0.22 | 0.10 | 0.08 | 1.0 |
| | 3/2 | 0.16 | 0.31 | 0.13 | (−0.07) | 0.02 | 0.60 | 0.32 | 0.79 | 0.27 | 3.1 | 0.35 | 0.25 | 0.25 | 0.22 | 1.2 |

## 5. Collisional rate constants

### *5.1. Results obtained by numerical solution*

Following the method described in section 2.2.2 we solved numerically (by means of a Digital PDP 11/40 computer) the normalized collisional rate constants, $k_{ij}/W$, from a set of $M(N-1)$ master equations of the type of eq. (2.5), using the data in tables 4 and 5. With regard to the large number of unknowns we first solved the equations under the assumption: $k_{ij} \equiv 0$ for jumps $|i-j| \geq m$ with $m = 2$. Next we solved the equations again, choosing successively $m = 3, 4, \ldots$ until the $k_{ij}$ values for small $|i-j|$ jumps converged while those for large jumps became vanishingly small or meaningless.

The normalized rate constants $k_{ij}/W$ are tabulated in tables 6 and 7 for the Ar- and $N_2$-diluted flame, respectively. Note that $i, j$ denote the numbering of the $(v', \Omega)$-levels in order of increasing energy in the rows and columns, respectively, so that each block corresponds to a particular $i \rightarrow j$ transition. We checked that an overall variation in $\xi$ (which was chosen equal to 2 in our $k_{ij}$ calculations; cf. eq. (2.4) and section 4) by a factor of 2 did not significantly affect the calculations. Also a stochastic variation of $\approx \pm 30\%$ in the individual $\delta n_Q$ values in tables 4 and 5 did not significantly affect the larger $k_{ij}$ values; only some smaller ones showed variations up to 50%.

### *5.2. Results obtained by successive approximation*

It appeared from the calculations mentioned above that collisional transitions between the doublet components with the same vibrational quantum number and those between neighbouring vibrational levels of the same doublet component are comparatively strong. Therefore we calculated the corresponding rate constants also more directly by the simplified method of successive approximation as described in section 2.2.3. The results of these calculations were initially normalized by dividing them by the *overall* depopulation rate constant $R$, while neglecting the dependence of $R$ on the number $j$ of the *final* level. In

Table 6

Calculated normalized rate constants $k_{ij}$ for binary collision-induced transitions from a level in the $i$th row to a level in the $j$th column in the Ar-diluted flame [a]

| v | | 0 | | 1 | | 2 | | 3 | | 4 | | 5 | | 6 | | 7 | |
|---|---|---|---|---|---|---|---|---|---|---|---|---|---|---|---|---|---|
| | Ω | 1/2 | 3/2 | 1/2 | 3/2 | 1/2 | 3/2 | 1/2 | 3/2 | 1/2 | 3/2 | 1/2 | 3/2 | 1/2 | 3/2 | 1/2 | 3/2 |
| 0 | 1/2 | | 1.28<br>1.29 | .15<br>.26 | .05 | 0.3 | | | | | | | | | | | |
| | 3/2 | 1.48<br>1.40 | | .24 | .01<br>0.9 | .01 | .00 | | | | | | | | | | |
| 1 | 1/2 | (1.28)<br>(1.0) | (−.50) | | 1.17<br>1.57 | .20<br>.39 | .01 | .02 | | | | | | | | | |
| | 3/2 | (−.46) | .90<br>.81 | .78<br>.82 | | .04 | .05<br>.13 | (−.03) | (−.01) | | | | | | | | |
| 2 | 1/2 | .05 | (−.08) | .89<br>.86 | (−.01) | | .89<br>1.09 | .09<br>.28 | .02 | (−.01) | | | | | | | |
| | 3/2 | | .27 | .14 | .16<br>.24 | .77<br>.88 | | .15 | .07<br>.13 | .03 | (−.03) | | | | | | |
| 3 | 1/2 | | | .30 | (−.24) | .50<br>.59 | .04 | | .42<br>.58 | .09<br>.18 | .03 | .02 | | | | | |
| | 3/2 | | | | .24 | (−.11) | .29<br>.42 | .42<br>.65 | | .12 | .06<br>.12 | .02 | (−.02) | | | | |
| 4 | 1/2 | | | | | .10 | (−.12) | .20<br>.35 | .16 | | .43<br>.56 | .05<br>.16 | .02 | .02 | | | |
| | 3/2 | | | | | | .13 | .06 | .15<br>.29 | .38<br>.48 | | .20 | .03<br>.06 | .02 | (−.02) | | |
| 5 | 1/2 | | | | | | | .13 | (−.11) | .31<br>.39 | .15 | | .34<br>.42 | .08<br>.16 | .01 | .01 | |
| | 3/2 | | | | | | | | .13 | .04 | .09<br>.15 | .29<br>.34 | | .11 | .03<br>.04 | .01 | .00 |
| 6 | 1/2 | | | | | | | | | .02 | (−.16) | (−.17)<br>(−.01) | .27 | | .32<br>.54 | .08<br>2.6 | .01 |
| | 3/2 | | | | | | | | | | .35 | .04 | .05<br>.11 | .12<br>.19 | | .08 | .02<br>.05 |
| 7 | 1/2 | | | | | | | | | | | .16 | (−.05) | .22<br>.30 | .09 | | .18<br>.27 |
| | 3/2 | | | | | | | | | | | | (−.04) | (−.04) | (−.06)<br>.00 | .25<br>.29 | |

[a] Whenever two figures are found in the same block, the upper one is obtained by numerical solution of the general rate equations (section 5.1) and the lower one by successive approximation of the simplified rate equations (section 5.2). All other figures are obtained by the former method. With both methods the same normalization $W = 1$ is applied. Negative values, which are physically meaningless, or very doubtful values are placed between parentheses but are listed to show the consistency limit of the calculations. Blocks far away from the diagonal were left blank because the corresponding figures appeared to be statistically insignificant. Estimated relative errors in the doubly, singly and not underlined (positive) figures are: > 25%, 10–25% and < 10%, respectively.

order to compare them with the $k_{ij}/W$ values calculated in section 5.1 we renormalized ($k_{ij}/R$) by multiplying them by ($R/W$), using the relation: $R = \Sigma_{j'} k_{jj'} + W$ [compare eq. (2.5) with eq. (2.9)]. $\Sigma_{j'} k_{jj'}/W$ was obtained by adding up the $k_{jj'}/W$ values appearing in the $j$th row in tables 6 or 7. It turned out that ($\Sigma_{j'} k_{jj'}/W + 1$) was, virtually, constant and equal to 1.6 ($\pm 0.1$) for the $N_2$-diluted flame, whereas it varied slowly between $\approx 2.8$ and 2.0 as a function of $j$ for the Ar-diluted flame. The renormalized ($k_{ij}/R$)($R/W$) values are also presented in tables 6 and 7 where they appear as the lower figure in the appropriate blocks.

### 5.3. Comparison of numerical and simplified methods of calculation

The results obtained from the simplified rate equations (see the lower figures in the appropriate blocks in tables 6 and 7) exceed those obtained numerically from the general rate equations, on the whole, by $\approx 50\%$. However, the results of both methods of calculation show mutual agreement as to the fulfilment of the detailed-balance relation (see section 6.1).

The systematically higher outcome of the simplified method of calculation might be caused by the fact that the underlying condition $k_{ij}/R \ll 1$ is not generally met in the Ar-flame where some $k_{ij}/W$ values are as large as 1.5 whereas $R/W$ is $\approx 2.5$ (see table 6 and section 5.2). This condition is somewhat better fulfilled in the $N_2$-flame where $k_{ij}/W$ is maximally but 0.5 and $R/W = 1.6$. We thus believe that the results obtained by the numerical method of calculation are the more realistic ones.

Table 7
Calculated normalized rate constants $k_{ij}$ for binary collision-induced transitions in the $N_2$-diluted flame [a]

| v | | 0 | | 1 | | 2 | | 3 | |
|---|---|---|---|---|---|---|---|---|---|
| | Ω | 1/2 | 3/2 | 1/2 | 3/2 | 1/2 | 3/2 | 1/2 | 3/2 |
| 0 | 1/2 | | .30<br>.46 | .04<br>.10 | .04 | .03 | | | |
| | 3/2 | .52<br>.66 | | .02 | .03<br>.08 | .01 | .04 | | |
| 1 | 1/2 | .19<br>.23 | .00 | | .30<br>.48 | .03<br>.07 | .02 | .00 | |
| | 3/2 | (−.02) | .22<br>.40 | .37<br>.56 | | .06 | .02<br>.06 | (−.01) | .01 |
| 2 | 1/2 | .08 | (−.05) | .12<br>.19 | .03 | | .26<br>.42 | .02<br>.06 | .01 |
| | 3/2 | | .14 | .00 | .15<br>.27 | .31<br>.45 | | .06 | .04<br>.10 |
| 3 | 1/2 | | | .13 | (−.03) | .18<br>.27 | .04 | | .25<br>.37 |
| | 3/2 | | | | .13 | .05 | .16<br>.31 | .40<br>.54 | |

[a] See footnote a) of table 6.

### 5.4. Internal consistency of the experimental results

The scatter between the individual normalized rate constants for a given type of transition at successive vibrational quantum numbers is clearly larger than anticipated from their estimated error limits. Also, some of the rate constants listed in tables 6 and 7 turn out to be negative. For the $N_2$-flame these negative values may easily be ascribed to statistical inaccuracies. For the Ar-flame a few unexpected large and systematically negative values appear, that cannot so easily be explained. We thus believe the data of the $N_2$-flame to be more reliable than those of the other flame. It is safe to regard differences up to 0.1 in the normalized rate constants as statistically insignificant.

## 6. Discussion and conclusions

### 6.1. Consistency check

We discuss here the validity of the assumptions made in our calculations and the internal consistency of the experimental results.

#### 6.1.1. The normalization rate constant W

The rate constants listed in tables 6 and 7 were normalized with respect to $W$ (see definition in section 2.2.1). We assumed that $W$ was the same

for all ($v$, $\Omega$)-levels investigated. In order to check this assumption and to convert the normalized rate constants to absolute values we derived $W$ from the *quantum efficiency of fluorescence* $Y$. We define $Y$ as the fraction of absorbed (laser) photons that is re-emitted in all directions in the same or other bands of the considered electronic transition (here: $A^2\Pi$–$X^2\Sigma$). In the steady-state, the rate of excitation from the ground state by photon absorption balances the rate of quenching plus radiative transitions back to the ground state. This balance leads to the following expression for $Y$ [1]:

$$Y = A/(A + k_q), \tag{6.1}$$

where $A$ is the Einstein coefficient for spontaneous emission and $k_q$ the rate constant for quenching collisions. Disregarding the existence of other excited electronic states in YO, we can equate $W$, virtually, to $(A + k_q)$. By determining $Y$ we thus find from eq. (6.1) an approximate value of $W$, $A$ being known.

Since the laser-excitation rate could not be directly measured (because of low absorption in the flame), we calculated $Y$ from our experimental data (for details see ref. [15]). In this calculation we used the effective spectral volume density of the wavelength-modulated laser beam, the known ratio of population increment $\delta n_i$ to thermal population $n_i^e$, the theoretical Boltzmann ratio of $n_i^e$ to the thermal ground-state population, and the theoretical relation between the Einstein coefficients for absorption and spontaneous emission. Pumping successively the vibrational levels $v_p = 0, \ldots, 4$ of either doublet state we found $Y$-values lying in the range $(1.2\text{–}2.4) \times 10^{-2}$ with both flames. Substituting the mean value $Y = 2 \times 10^{-2}$ and $A = 3 \times 10^7\ s^{-1}$ in eq. (6.1) we found $W = (1.6 \pm 50\%) \times 10^9\ s^{-1}$ for both flames. By multiplying all figures in tables 6 and 7 by this common factor we get the *absolute* rate constants.

The absence of a pronounced dependence of $Y$ on the pumped level supports the assumption made in section 5 that $W$ is independent of $i$ (at least up to $i = 10$) in both flames. We note in this connection that, roughly speaking, half of the total fluorescence from the $A^2\Pi$ doublet states is emitted from the pumped level. A pronounced dependence of $W$ on $i$ would thus manifest itself as a dependence of $Y$ on the pumped level.

Since $Y$ appears to be small compared to unity, the relative population distribution in the $A^2\Pi$ doublet states is *collision-dominated* (i.e. $k_q \gg A$). This supports the assumption made in sections 2 and 3 that, in the absence of laser excitation, the $A^2\Pi$ levels are populated according to the Boltzmann law.

### 6.1.2. Detailed-balance test

If the rate constants are truly thermal and correctly measured, the ratio $k_{ij}/k_{ji}$ should obey the detailed-balance (DB) relation given by eq. (2.1) in combination with eq. (2.8). Table 8 lists weighted average ratios of the normalized rate constants for exoergic and inverse endoergic pure $|\Delta\Omega| = 1$ or $|\Delta v| = 1$ transitions *. We note that the normalization rate constant $W$ drops out in these ratios. The theoretical ratios are also listed.

The experimental ratios obtained by the general and the simplified methods are in mutual agreement within their combined error limits. The two experimental $k_{ij}/k_{ji}$ ratios for pure mixing ($|\Delta\Omega| = 1$; $\Delta v = 0$) transitions agree within 20% with the theoretical ratio in the $N_2$-flame. In the Ar-flame the experimental ratios for the same process are systematically less by at least 20% than the theoretical ratio. On the other hand, the experimental ratios for the pure $|\Delta v| = 1$ transitions tend to exceed the theoretical ratios.

These deviations can hardly be explained by a systematic but unnoticed dependence of $W$ on $v$ or $\Omega$ [15]; in addition a dependence of the quenching rate constant $k_q$ (which is contained in $W$) on spin–orbit coupling is not expected for Ar as collision partner; see also the end of section 6.1.1. (for $N_2$ such dependence can be excluded because of the good agreement between the experimental and theoretical ratios for pure mixing collision.)

A more intriguing question is whether the collisional rate constants derived from the *time-averaged* population increments $\delta n_i$ with modulated

* We speak here of an "exoergic" or "endoergic" transition when the internal energy of the final ($v$, $\Omega$)-level is lower or higher than that of the initial level. The *rotational* energy is *not* included in this definition of internal energy.

Table 8
$k_{ij}/k_{ji}$ ratios [a]

| | $N_2$-flame | | | Ar-flame | | |
|---|---|---|---|---|---|---|
| | GEN | SIMP | TH | GEN | SIMP | TH |
| mixing | 1.4±0.2 | 1.3±0.2 | 1.31 | 0.9±0.2 | 0.9±0.2 | 1.29 |
| $\|\Delta v\| = 1$ | – | 3.5±1 | 1.69 | 3.5±1.5 | 2.2±0.5 | 1.64 |

[a] Weighted average values of ratios of the rate constants $k_{ij}$ and $k_{ji}$ for pure doublet mixing and pure $|\Delta v| = 1$ transitions. Experimental values obtained by numerical solution of the general rate equations and by solution of the simplified rate equations are listed under GEN and SIMP, respectively. Theoretical ratios calculated from the detailed-balance relation are listed under TH.

laser wavelength (see section 3.1.2) are truly *thermal*, even if the time-averaged rotational distributions are thermal. At each moment during the wavelength-modulation period the rotational distribution in the pumped ($v$, $\Omega$)-level has been shown to be non-thermal [14,15]. If the rate constants for collisional transitions to other ($v$, $\Omega$)-levels depend on the initial rotational quantum number (cf. section 6.2.4), the momentaneous rate constants for ($v$, $\Omega$)-transitions are non-thermal, too. However, one can prove that the laser-induced increments in ($v$, $\Omega$)-level populations when averaged over time are strictly connected by thermal rate constants when the time-averaged rotational distributions are thermal. This proof is based on the linearity of the complete relaxation matrix which includes transitions between specific rotational levels [15]. So the deviations from the DB ratio observed in table 3 cannot be ascribed to our laser-wavelength modulation technique as such.

The deviations from the DB ratios might be caused by departures of the time-averaged rotational distribution in the excited state from a Boltzmann distribution. It is true that we found the shapes of the P-, Q- and R-branches in the time-averaged fluorescence spectrum to conform grossly to the corresponding shapes in the thermal emission spectrum (see section 3.2). However, slight, unnoticed departures from a Boltzmann distribution, especially at high $J$-levels, might have a noticeable effect on the measured rate constants if the rate constants for *specific* rovibronic transitions depend markedly on $J$. The dependence on initial $J$-value may be different for pure mixing and pure vibrational transitions; it may also be different for $N_2$ and Ar as collision partner. This could explain why in the $N_2$-flame the experimental ratios do conform to the DB ratios for pure mixing collisions but not for pure vibrational transitions, and why in the Ar-flame deviations (of opposite sign!) were found for both transitions.

### 6.2. Conclusions

#### 6.2.1. General trends in the experimental rate constants

Since the normalization rate constant $W$ has the same, constant value (within 50%) in both flames, the gross trends noted in tables 6 and 7 for the normalized rate constants apply also to their absolute values.

In both flames the rate constants for exoergic pure doublet-mixing, pure $\Delta v = -1$ and pure $\Delta v = -2$ transitions decrease, on the average, in this order. The rate constants for *combined* mixing and vibrational transitions are comparatively small.

No systematic dependence on $\Omega$ was found for pure $\Delta v = -1$ transitions.

The rate constants for pure doublet-mixing collisions (up to $v = 3$) are systematically larger in the Ar-flame than in the $N_2$-flame.

The probability of an $\Omega$- and/or $v$-changing collision within the A state is less than that of a quenching collision in the $N_2$-flame (because $k_{ij}/W \leq 0.4$ and $W \approx k_q$; see section 6.1.1). In the Ar-flame pure mixing collisions in the $v = 0$ state are even more probable than quenching collisions.

Since our flames contained about equal concentrations of $H_2O$ and $N_2$ *or* Ar, we cannot associate the measured rate constants with a specific collision partner. By keeping the absolute $H_2O$ concentration the same in the Ar- and $N_2$-

flame, we can, however, ascribe the *differences* in rate constants to differences in Ar and $N_2$ as collision partner. We note that it was not possible to vary the $H_2O$:Ar (or $N_2$) concentration ratio over a significant range without drastically changing the flame temperature. Anyway, the similarity in the values of $W (= k_q)$ found in the two flames points to Ar being as effective as $N_2$ in quenching the $A^2\Pi$ state. Disregarding tentatively $H_2O$ as collision partner we calculate an upper limit of $= 40$ Å$^2$ for the effective cross sections of $N_2$ and Ar for inducing ($\Omega = 3/2 \rightarrow 1/2$; $v = 0$) transitions.

*6.2.2. Multiple-collision conditions*

Since many of the normalized rate constants $k_{ij}/W$ are of order unity, molecules pumped into the $A^2\Pi$-state have a good chance to undergo more than one VET or doublet-mixing collision during their lifetime ($= W^{-1}$). Multiple collisions are also manifest from the observed population of levels that lie far away from the pumped level (see tables 4 and 5). We note that the probability of a large $|i - j|$ jump in a single collision appeared to be comparatively small. Multiple collisions lead ultimately to the observed partial Boltzmann population distribution among the levels far above the pumped level.

The stationary fluorescence method described in this paper has thus proved to be capable, in principle, of yielding (normalized) rate constants for *single*-collision *transitions* between specific ($v$, $\Omega$)-levels under *multiple*-collision *conditions*. The toll paid for this is the complexity of solving a set of simultaneous linear rate equations.

*6.2.3. Detailed-balance relation*

The measured rate constants for ($v$, $\Omega$)-transitions are weighted averages over the relative velocity as well as over the initial rotational energy distribution. There is no doubt that the distribution of the relative velocities conforms to Maxwell's law in our flames. If the rate constants for ($v$, $\Omega$)-transitions depend markedly on initial $J$-value (cf. section 6.2.4.), the measured, averaged rate constants have an unambiguous (be it incomplete) physical meaning only if the rotational energy distributions conform to Boltzmann's law. If the rate constants for ($v$, $\Omega$)-transitions would be independent of initial $J$-value, the physical meaning of the measured rate constants is not only unambiguous but also complete. In both cases we can unambiguously identify the measured values as *thermal* rate constants. They are exactly reproducible (at given perturber density) if the translational as well as rotational degrees of freedom conform to Maxwell–Boltzmann equilibrium. This adds to the practical significance of the measured rate constants in work with gases in which these degrees of freedom are equilibrated.

A sensitive check on the occurrence of thermal rate constants is the detailed-balance test (see section 6.1.4.). The DB relation for the translationally and rotationally averaged rate constants holds strictly irrespective of the actual jumps in translational or rotational energy that accompany any ($v$, $\Omega$)-transition. (These jumps may easily outweigh the jump in vibronic energy as the f.s. splitting and the vibrational quantum are $= \frac{1}{4}k_BT$ and $\frac{1}{2}k_BT$, respectively.) Of course, the measured rate constants yield no detailed information about these combined jumps in internal and translational energy. Also, the dependence of the thermal rate constants on temperature has not been investigated. (The slight difference of $\approx 100$ K in flame temperatures was considered as insignificant.)

One should be cautious in relating a priori the conjugated rate constants $k_{ij}$ and $k_{ji}$ for inelastic collisions by detailed-balance. This applied especially to cases when the measured rate constants are weighted averages over an internal (here: rotational) degree of freedom that is not specified in the experiment. We recommend here that the detailed-balance relation be applied – in contrast to common usage – as an ex postfacto check on the experiments. The close agreement between the experimental and theoretical $k_{ij}/k_{ji}$ ratios for pure doublet-mixing collisions in the $N_2$-flame verifies that these rate constants are close to their thermal values. This agreement also substantiates the applicability of our experimental method.

*6.2.4. Comparison with other experimental and theoretical data*

Only recently quantitative data have become available that clearly show the pronounced depen-

dence of the rate constant for collisional $(v_i, J_i) \rightarrow (v_f, J_f)$ transitions on initial and final rotational quantum numbers, $J_i$ and $J_f$ [18]. These experiments were performed on $Li_2(A^1\Sigma^+)$ molecules perturbed by Xe atoms in a cell, using laser-induced fluorescence spectroscopy. The total rate constant obtained by summation over $J_f$ appeared to depend markedly on $J_i$. For given $J_i$, the distribution over $J_f$ was strongly peaked, especially so for $v_f = v_i - 1$ transitions. Experiments with other noble gases have yielded similar results, except for He [19]. The authors have concluded that to a large extent the sum of vibrational and rotational energy is conserved in vibrationally inelastic collisions. The $J_i$-dependence may explain, by analogy, some of the features found in our work (see sections 6.1.4. and 6.2.3.).

The conclusions in ref. [18] are supported by Monte Carlo quasiclassical trajectory calculations on Ar + HF ground-state collisions [20]. In these calculations, based on a modified infinite-order-sudden-approximation, a diatomics-in-triatomic sum potential was used:

$$V(r_{HF}, r_{ArH}, r_{ArF}) = V_M(r_{HF}) + V_{LJ}(r_{ArH}) + V_{LJ}(r_{ArF}),$$

where $V_M$ denotes a Morse potential and $V_{LJ}$ a Lennard-Jones potential. Such calculations on YO(A $^2\Pi$) colliding with Ar are, however, hampered by lack of knowledge of the (excited) Y–Ar and O–Ar potentials.

As far as we know, in only one other experiment qualitative features in the rotational, vibrational and intramultiplet transfer have been noticed [7]. These observations were made in a gas flow of Ar with YO vapour at low pressure and low temperature. Collisions of Ar atoms with YO(A $^2\Pi_{3/2}$, $v = 1$) molecules, excited by a narrow-band dye laser, resulted in a population of the (A $^2\Pi_{1/2}$, $v = 2$) level which *exceeded* that of the (A $^2\Pi_{1/2}$, $v = 1$) level. There is a seeming contradiction between this and our results. This may be explained by considering that in the former experiment the rotational distribution (not specified by the author) in the pumped band is probably peaked, whereas in our experiments this distribution was fairly equilibrated. This again points to a marked dependence of the rate constant on $J_i$.

The larger rate constants obtained with Ar compared to $N_2$, as found by us, are in agreement with the measurements of Edelstein and Huestis [12] on the excited doublet-levels of BaCl. Intramultiplet transfer from (C $^2\Pi_{3/2}$, $v = 0$) to (C $^2\Pi_{1/2}$, $v = 0, 1, 2$) was observed with Ar, He and $N_2$ as perturber. Also in this case the rate constants obtained with Ar were larger (by about a factor 3) than with $N_2$. Our upper limit of 40 Å$^2$ for the intramultiplet transfer cross sections is three times larger than the cross section for the corresponding process found with BaCl.

The cross sections for intramultiplet transfer from the CdH(A $^2\Pi_{3/2}$, $v = 0$) level to the lower lying (A $^2\Pi_{1/2}$) level with Ar and He have been found to be smaller than 5 Å$^2$ [11]. This low value might be due to the much greater level separations.

It is also interesting to compare the cross sections for pure doublet mixing in YO with those found in alkali atoms. The Cs(6 $^2$P) doublet separation ($\approx 550$ cm$^{-1}$) is about equal to that in YO(A $^2\Pi$) (see table 1). With $N_2$ as perturber the exoergic Cs mixing cross section has been measured to be 55 Å$^2$ in a flame [21]. With Ar the corresponding cross section, measured in a vapour cell, is vanishingly small ($\ll 1$ Å$^2$) [22]. The cross sections for Cs and YO with $N_2$ agree mutually as to order of magnitude, but not so with Ar. The theoretical models invoked to explain the very small mixing cross section for Cs with Ar [1] are thus not applicable to the case of YO.

### 6.3. Some by-products

In our experiments we could not detect any thermal emission or laser-induced fluorescence from the A′ $^2\Delta$ state to the ground state, whereas in chemiluminescence experiments at low pressure this transition has been detected [17]. Estimating mixing coefficients between the A′ $^2\Delta$ and A $^2\Pi$ quantum states an *Einstein transition probability* ratio of $2 \times 10^{-2}$ has been calculated in this paper for the (A′ $^2\Delta_{3/2}$, $v' = 0 \rightarrow$ X $^2\Sigma$, $v'' = 0$) and (A $^2\Pi_{3/2}$, $v' = 0 \rightarrow$ X $^2\Sigma$, $v'' = 0$) transitions. We must conclude from our intensity-calibrated recordings of the thermal emission spectrum that this ratio cannot exceed $2 \times 10^{-4}$, assuming thermal equilibrium in the $N_2$-diluted flame. There is

thus a discrepancy of (at least) two orders of magnitude.

A second by-product, connected with our Q-branch correction (section 3.2), concerns the *partial parity conservation* of the rotational levels in the pumped vibrational level $p$. The symmetry properties of rotational levels in diatomics are designated by distinguishing between e- and f-levels, depending on the symmetry of the molecular wavefunction with respect to inversion of the space-fixed reference system. Accordingly, e-levels have parity $-(-1)^{J+1/2}$, whereas f-levels have parity $+(-1)^{J+1/2}$. In the case of Q-branch excitation of YO($\Pi \leftarrow \Sigma$), only f-levels can be populated [5,15,23]. If no e–f transfer collisions occur, lines originating from e-levels will thus be missing in the fluorescence spectrum. As a consequence, the P:Q:R fluorescence intensity ratio will be 1:3:0 [15,24] instead of 4:3:1 as expected theoretically in thermal equilibrium (table 2). We recall that the latter ratio applies to our thermal emission spectrum. The actually observed fluorescence intensity ratios belonging to Q-branch excitation are 1.7:3:0.4 and 1.3:3:0.3 in the Ar- and $N_2$-diluted flame, respectively (see section 3.2). Total preservation of e/f symmetry in YO ($A^2\Pi$) has been observed by Linton [7] at much lower Ar pressure. An interpretation of this propensity rule has been given by Gottscho [25], whereas Alexander [26] has presented a full close-coupling theory of this rule for a collision between an $^2\Pi$ molecule (Hund's case a) and a structureless target particle. He has shown that when a sudden-approximation formulation of the collision dynamics or a Born distorted-wave approximation is appropriate, rotationally inelastic transitions conserving this symmetry index will be strongly favoured at large values of total internal angular momentum. The theory also shows that this propensity rule does not hold for collisional transitions between $^2\Pi_{3/2}$ and $^2\Pi_{1/2}$ states. The condition of large total internal angular momentum is well met at the temperature of our flames. We conclude that the above fluorescence intensity ratios found in our flames for the pumped vibronic levels with Q-branch excitation do not much deviate from the ratio predicted if e/f parity-index were preserved. The relatively small deviations might be due to excitation of molecules with low $J$-values and/or to successive collisions transferring pumped YO molecules to other vibronic levels and back into the pumped level. In this connection we recall that the fluorescence intensity ratios from the other, collisionally repopulated vibronic levels agree with those in thermal emission. We can conclude therefrom that doublet-mixing or vibrationally inelastic collisions do not preserve the parity-index e/f. The former conclusion is supported by theory [26].

## Acknowledgement

We are much indebted to Dr. B.P. van Eijck, who developed the computer program and performed the calculations of relative rate constants.

## References

[1] C.Th.J. Alkemade, Tj. Hollander, W. Snelleman and P.J.Th. Zeegers, Metal vapours in flames (Pergamon Press, Oxford, 1982).
[2] R.G. Gordon and J.I. Steinfeld, in: Molecular energy transfer, eds. R. Levine and J. Jortner (Wiley, New York, 1976) p. 67.
[3] K. Liu and J.M. Parson, J. Chem. Phys. 67 (1977) 1814.
[4] U. Uhler and L. Åkerlind, Arkiv Fysik 19 (1961) 1.
[5] A. Bernhard, R. Bacis and P. Luc, Astrophys. J. 277 (1979) 338.
[6] C.L. Chalek and J.L. Gole, Chem. Phys. 19 (1977) 59.
[7] C. Linton, J. Mol. Spectry 69 (1978) 351.
[8] K. Sakurai, S.E. Johnson and H.P. Broida, J. Chem. Phys. 52 (1970) 1625.
[9] R.A. Gottscho, R.W. Field, R. Bacis and S.J. Silvers, J. Chem. Phys. 73 (1980) 599.
[10] Th.G. Cats, J.G.M. Kuerten, M.I.M. Scheerboom, C.W.J.M. Klaasen, H.A. Dijkerman and C.Th.J. Alkemade, Chem. Phys. Letters 105 (1984) 347.
[11] J. Dufayard and O. Nédélec, Chem. Phys. 71 (1982) 279.
[12] S.A. Edelstein and D.L. Huestis, J. Chem. Phys. 70 (1979) 131.
[13] S.A. Edelstein, J. Chem. Phys. 70 (1979) 591.
[14] T. Wijchers, H.A. Dijkerman, P.J.Th. Zeegers and C.Th.J. Alkemade, Spectrochim. Acta 35B (1980) 271.
[15] T. Wijchers, Ph.D. Thesis, University of Utrecht, The Netherlands (1981) (in Dutch with abbreviated version in English; available on request).
[16] W.F. Meggers and J.A. Wheeler, J. Res. Natl. Bur. Std. US 6 (1931) 239.
[17] C.L.Chalek and J.L. Gole, J. Chem. Phys. 65 (1976) 2845.

[18] K.L. Saenger, N. Smith, S.L. Dexheimer, C. Engelke and D.E. Pritchard, J. Chem. Phys. 79 (1983) 4076.
[19] D.E. Pritchard, private communication.
[20] D.L. Thompson, J. Chem. Phys. 76 (1982) 5947.
[21] P.L. Lijnse, P.J.Th. Zeegers and C.Th.J. Alkemade, J. Quant. Spectry. Radiative Transfer 13 (1973) 1301.
[22] M. Czajkowski, D.A. McGillis and L. Krause, Can. J. Phys. 44 (1966) 741.
[23] G. Herzberg, Molecular spectra and molecular structure, Vol. 1. Spectra of diatomic molecules (Van Nostrand, Princeton, 1950; reprint 1964).
[24] J. Kovács, Rotational structure in the spectra of diatomic molecules (Hilger, London, 1969);
T.L. Earls, Phys. Rev. 48 (1935) 423.
[25] R.A. Gottscho, Chem. Phys. Letters 81 (1981) 66.
[26] M.H. Alexander, J. Chem. Phys. 76 (1982) 5974.